Controlling interfacial exchanges in liquid phase bonding enables formation of strong and reliable Cu–Sn soldering for high-power and temperature applications

Jean-François Silvain, Loïc Constantin, Jean-Marc Heintz, Sylvie Bordère, Lionel Teulé-Gay, Yongfeng Lu, Jean-Luc Diot, Renaud de Langlade, Emilien Feuillet

Controlling interfacial exchanges in a liquid phase bonding enables forming strong and reliable Cu-Sn soldering for high-power and temperature applications

Jean-François Silvain[a,b,], Loic Constantin[b], Jean-Marc Heintz[a], Sylvie Bordère[c], Lionel Teule-Gay[a], Yong Feng Lu[b], Jean-Luc Diot[d], Renaud de Langlade[d], Emilien Feuillet[e]*

[a] CNRS, Univ. Bordeaux, Bordeaux INP, ICMCB, UPMR 5026, F-33608 Pessac, France

[b] Department of Electrical and Computer Engineering, University of Nebraska-Lincoln, Lincoln, Nebraska, 68588-0511, United States

[c] CNRS, Univ. Bordeaux, Bordeaux INP, I2M, UPMR 5295, F-33608 Pessac, France

[d] Composite Innovation, 2 allée du Doyen Brus, 33600 PESSAC (France)

[e] Innoptics, rue François Mitterrand, 33400 TALENCE (France)

Abstract: Developing solder joints capable of withstanding high-power density, high-temperature, and significant thermomechanical stress is essential to further develop electronic devices performances. This study demonstrates an effective route of producing dense, robust, and reliable high-temperature Cu-Sn soldering by modifying the interfacial exchange during a transient liquid phase bonding (TLP) process. Our approach relies thus on altering internal phenomena (diffusion and transport of reactive species) rather than classical external TLP bonding parameters (e.g., time, temperature, and pressure). By adding a Cu_3Sn coated layer between Cu and Sn before the TLP process, a fast dissolution of Cu in liquid Sn is achieved, altering undesired Cu_6Sn_5 scallop grains impingement and promoting their uniform growth within the liquid. A bonding and pore formation mechanism of the solder with or not the Cu_3Sn coated layer is proposed based on experimental and theoretical analysis. The developed TLP joint possesses a shear stress resistance of more than 80 MPa with a thermal cycle endurance

superior to 1200 (-45 to 180 ºC), making it highly reliable compared to a classical solder joint with shear and thermal cycling resistance of 45 MPa and 500, respectively. The developed approaches provide, thus, an easy, affordable, and scalable method of producing high-temperature and durable Cu-Sn joint for high-power module applications.

Keywords: Transient liquid phase bonding; Intermetallic; Cu-Sn; Diffusion; Mechanical characterization.

Introduction

The current trend in power electronics requires using solder technologies that can handle high power densities, high junction temperatures (superior to 200 °C), and withstand significant thermomechanical stresses during multiple on/off cycles [1]. Yet, classical packaging technologies utilize soft soldering and wire bonding, which suffer from low thermomechanical resistance, limiting the power module performances [2].

In the late 1950s, J. F. Lynch et al. introduced the transient liquid phase (TLP) bonding as a hybrid process, combining diffusion bonding and brazing [3-4]. Since then, the TLP bonding has drawn significant consideration as a promising method of producing high-temperature solder joints [5-8]. The TLP bonding relies on using an intermetallic compound (IMC) as a bonding medium. During the high-temperature bonding, the IMC turns liquid, which is then progressively consumed. The TLP process uses a binary system composed of either two metals or metal alloys with different melting points. A well-known system is the copper-tin (Cu-Sn), where Sn is the low-melting-point interlayer, inserted between two high-melting-point Cu layers. The Cu-Sn system has been intensively studied due to its affordability, the low Cu-Sn melting points, and the widespread usage of Cu in electronic packaging [9]. According to the Cu-Sn phase diagram, Cu_6Sn_5 and Cu_3Sn are the two main IMCs which form and grow under the TLP bonding conditions [10-11]. In addition, if Sn fully transforms into Cu_3Sn, the solder joint becomes thermodynamically stable (up to 350 °C). Also, Cu_3Sn has a much higher remelting temperature (676 °C) than the process temperature making the Cu-Sn system of great interest [12].

Previous reports have shown that the growth kinetics and morphology evolutions of Cu-Sn IMCs during TLP soldering depend upon the process parameters (e.g., heating rate, bonding temperature, compressive stress, etc.), and the initial thickness of the Sn interlayer [13-14]. W.L. Chui et al. demonstrated that from 240 °C to 280 °C and in the early stages of the process,

the growth of Cu_6Sn_5 dominates [14]. Next, when the liquid Sn ($Sn_{(l)}$) is fully consumed, the Cu_3Sn layer grows at the expense of the previously formed Cu_6Sn_5. It was observed that the Cu_6Sn_5 grows into a rounded grains morphology called scallops from both Cu/Sn bonding interfaces [15]. Later, such grains development led to a Cu_6Sn_5 impingement before the total Sn consumption, thus forming pores in the solder joint [2, 8, 16]. Naturally, pores degrade the IMC's thermal and mechanical properties and deteriorate its reliability [17]. It has been shown that high temperature, fast heating rate, thin Sn foil, and intimate contact between layers help to decrease the number of pores but cannot suppress them [13, 14]. Recently, O. Mokhatari reviewed the current TLP soldering state-of-the-art and concluded that voids' formation is yet to be understood during the process but must be prevented and reduced to enhance the attractiveness of the method and effectiveness of the solder joint [18]. Although these results, forming pore-free, robust, and durable high-temperature and power IMC joints remains challenging.

Here, instead of simply relying on external TLP bonding parameters (e.g., temperature, time, and pressure) to fabricate void-free, strong, and reliable Cu-Sn solder joints, we proposed to modify the interfacial exchange between Cu and a $SnAg_{3.8}Cu_{0.7}$ (SAC) filler metal. As previously reported, adding a layer between a metal and filler metal influences the nucleation, growth, and morphology of IMCs [19, 20]. Therefore, in a similar fashion, we altered the growth of Cu_6Sn_5 scallops by inserting a Cu_3Sn coated layer between Cu and SAC during the TLP bonding. We showed that the deposition of a Cu_3Sn layer between Sn and Cu before the TLP bonding process allows suppressing grains impingement, leading to a pore-free Cu-Sn solder joint. A bonding and pore formation mechanism of the solder having or not the Cu_3Sn coated layer is proposed based on microstructural, elemental, chemical analysis, and previously reported kinetic and thermodynamic simulation diffusion of the TLP process [8]. Finally, the mechanical and thermomechanical properties of the bonded materials having the Cu_3Sn coated

layer were studied and compared to a classical SAC solder joint. Adding a Cu_3Sn layer enables modifying internal phenomena during the bonding process and holds great promise to remove the bottleneck of the TLP method.

Experimental part

Deposition of the Cu_3Sn coated layer: The deposition of a thin Sn layer on top of the Cu substrates (Goodfollow™, 99.9 purity, 30×30×3 mm^3) was carried out by radiofrequency sputtering (Plassys™ MP 700 at ambient temperature). The Sn target (Neyco™ target Sn, 99.99%) was powered by a 13.56 MHz radiofrequency supply with a fixed value of 15 W. Every 30 min, the deposit was impinging by Argon (Ar) ions (Anatech Ion gun) during 30 s with an accelerator voltage of -50 V. The deposition rate was estimated to be about 0.4 μm/h. The coated Sn film was then annealed at 250 °C for 10 min under a reducing atmosphere composed of Ar and dihydrogen (H_2, 5%), which gave rise to a Cu_3Sn layer on top of the Cu substrate.

Formation of the bonded assembly: Bonded materials were fabricated by combining a substrate of Cu or Cu/carbon fibers (CFs) composites having or not a Cu_3Sn coated-layer with a $SnAg_{3.8}Cu_{0.7}$ solder sheet (SAC, Materon™, thickness = 20 μm). The Cu composites were fabricated using a uniaxial hot pressing at 650 °C under 50 MPa for 30 min. More information on the Cu/CF composites fabrication can be found elsewhere [18]. A Lamination Press (MTI Corporation™ VHP-5T-4 500 °C) was used to combine the different layers. The applied pressure and temperature were fixed to 10 kPa and 270 °C, respectively.

Mechanical and thermomechanical testing of the Cu-Sn joint: The double notch shear (DNS) test was selected to measure the mechanical properties of the IMCs because of its simplicity of implementation. The DNS test follows the ISO standard 11003-2 using an Instron machine (Model 3369) with a 1 mm/min displacement speed and a maximum loading charge of 50 kN.

The notch's diameter and length were fixed to 0.3 and 2.5 mm, respectively, with a distance between two notches of 2.5 mm. The thickness and size of the Cu substrate were 5 and 15 mm, respectively. The deformation behavior and stresses were simulated by a stress analysis model using COMSOL® finite element software. The Cu substrates were modeled with an elastoplastic equation, whereas the IMC joint stays in its elastic domain. The parameters used for that simulation are the following: density, d_{Cu} = 8960 kg/m^3, d_{IMC} = 8900 kg/m^3 ; Young modulus E_{Cu} = 100 GPa, E_{Cu} = 110 GPa ; Poisson coefficient, ν_{Cu} = 0.35, ν_{Cu} = 0.33 and yield point; σ_{Cu} = 100 MPa.

The thermomechanical of the bonded layer were evaluated using in a climatic chamber (CTS Clima Temperatur Systeme^{TM}, T-40/25). The assemblies were inserted in the chamber and subjected to open-air passive thermal cycles. A cycle duration was set to 120 min, with a first plateau at 180 °C for 20 min and a second plateau at -45 °C for 20 min.

Microstructural characterization: The microstructure of the joints was characterized using scanning electron microscopy (SEM, VEGA II SBH, TESCAN^{TM}). Auger electron spectroscopy (AES) was performed using a Nano sonde AUGER PHI^{TM} 710 equipment with an analysis diameter of about 50 nm. The SAC was etched with a solution of hydrochloric acid and water (50:50) for 10 s.

Results and discussions

1. Preparation of the Cu_3Sn layer on Cu substrates.

The Cu-SAC system undergoes various phases and microstructural evolutions during the TLP soldering process. As observed by others, Cu_6Sn_5 forms first, which then transforms into Cu_3Sn [21]. However, the Cu_6Sn_5 grows in the form of scallop, inducing grains impingement and pores in the solder layer, thus deteriorating its mechanical and thermomechanical properties. It has been reported that during a wettability measurement, a Cu_3Sn layer modified the nucleation,

growth, and morphology of Cu_6Sn_5 scallops when inserted between Cu and Sn [20]. Particularly, in the presence of a Cu_3Sn layer, the Cu_6Sn_5 phase preferentially grows inside the $Sn_{(l)}$ rather than at the $Cu/Sn_{(l)}$ interfaces. In addition, Cu_3Sn has a high melting point compared to Sn or SAC, making it a pertinent candidate to alter the interfacial exchange. Likewise, we synthesized a Cu_3Sn layer between Cu and SAC to suppress the scallops grain impingement. The Cu_3Sn layer was obtained by first depositing a thin Sn layer onto a Cu substrate, followed by an annealing treatment at 250 ºC for 10 min, as illustrated in **Figure 1a**. The thickness of the Cu_3Sn layer was set to 1 µm to avoid forming a thick seal. **Figure 1b** shows a top view of the Cu_3Sn film after the annealing treatment. It can be observed that the Cu substrate is homogeneously coated with Cu_3Sn, having a grain size of about 1 µm. **Figure 1c** shows a cross-sectional view of the Cu_3Sn film on the Cu substrate, where a significantly rough film is obtained.

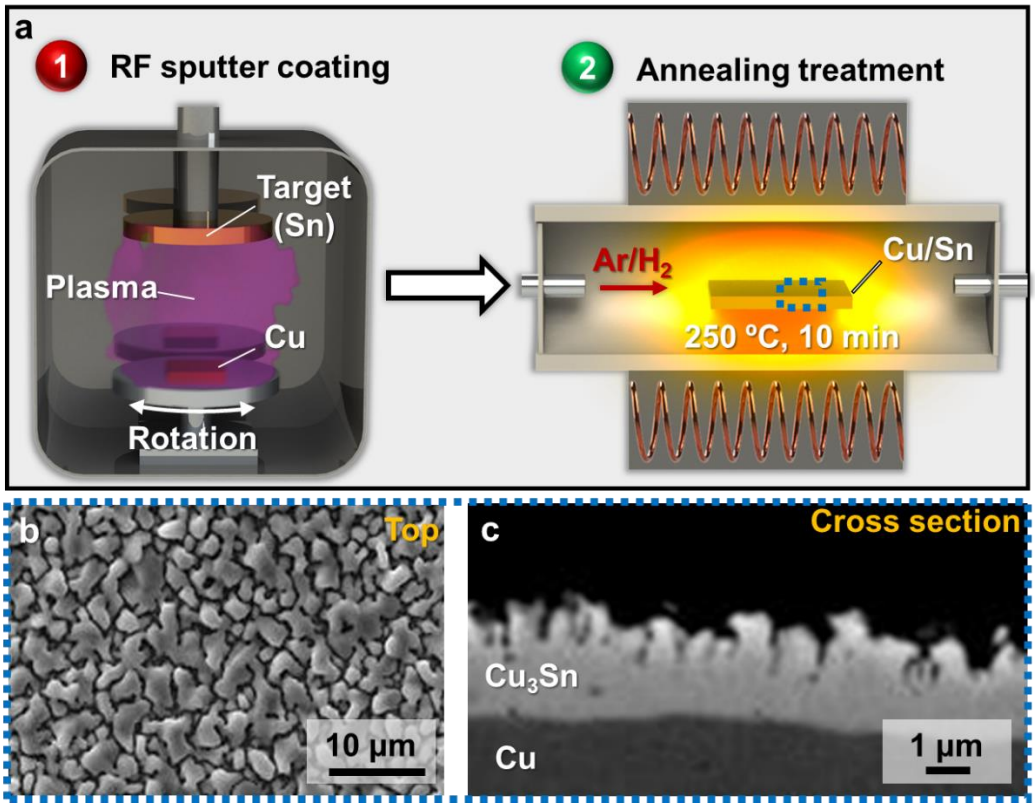

Figure 1. (a) Illustration of the Cu_3Sn coated layer synthetized on Cu. SEM micrographs of the Cu_3Sn, **(b)** top, and **(c)** cross-sectional views.

2. Effect of the Cu_3Sn coated layer on the Cu/SAC soldering microstructure.

A SAC filler metal layer was used to bond two Cu substrates having or not the Cu_3Sn coated layer, as illustrated in **Figure 2a**. Once bonded via the TLP process, at 270 ºC for 120 min and under 10 kPa, the samples were cut and mechanically polished for microstructural observations. As can be observed in the low magnifications backscattered electron (BSE) micrographs in **Figure 2b,** the bonded Cu-SAC-Cu has numerous macropores along the solder joint. **Figure 2c** shows higher magnification BSE micrographs of the Cu-SAC-Cu bonded layer where three-color contrasts can be identified. In this detection mode, Cu appears darker than Cu_3Sn, which is darker than Cu_6Sn_5. The BSE observations suggest, thus, the formation of a thick Cu_6Sn_5 layer and thin Cu_3Sn interphases as a result of the Cu and SAC reaction. An AES line profile was performed across the bonding layer to confirm the formation of Cu_6Sn_5 and Cu_3Sn phases, as shown in **Figure 2d**. The measured Cu and Sn atomic percentages (at.%) suggest the following sequence: Cu, Cu_3Sn, Cu_6Sn_5, Cu_3Sn, and Cu and corroborate the BSE observations. An equivalent microstructure is also obtained on the Cu-Cu_3Sn-SAC-Cu_3Sn-Cu sample, as shown in **Figure 2e** and **Figure 2f**. The volume fractions of the Cu_6Sn_5 and Cu_3Sn phases appear similar regardless of the Cu_3Sn coated layer presence and measured to be about 90 and 10 vol.%, respectively. However, in the absence of the Cu_3Sn coated layer, macropores formed inside the Cu_6Sn_5 phase (**Figure 2b and Figure 2c),** while only a few micropores formed close to the Cu_3Sn interphases with a Cu_3Sn coated layer as can be seen on the low and high magnification SEM in **Figure 2e** and **Figure 2f,** respectively.

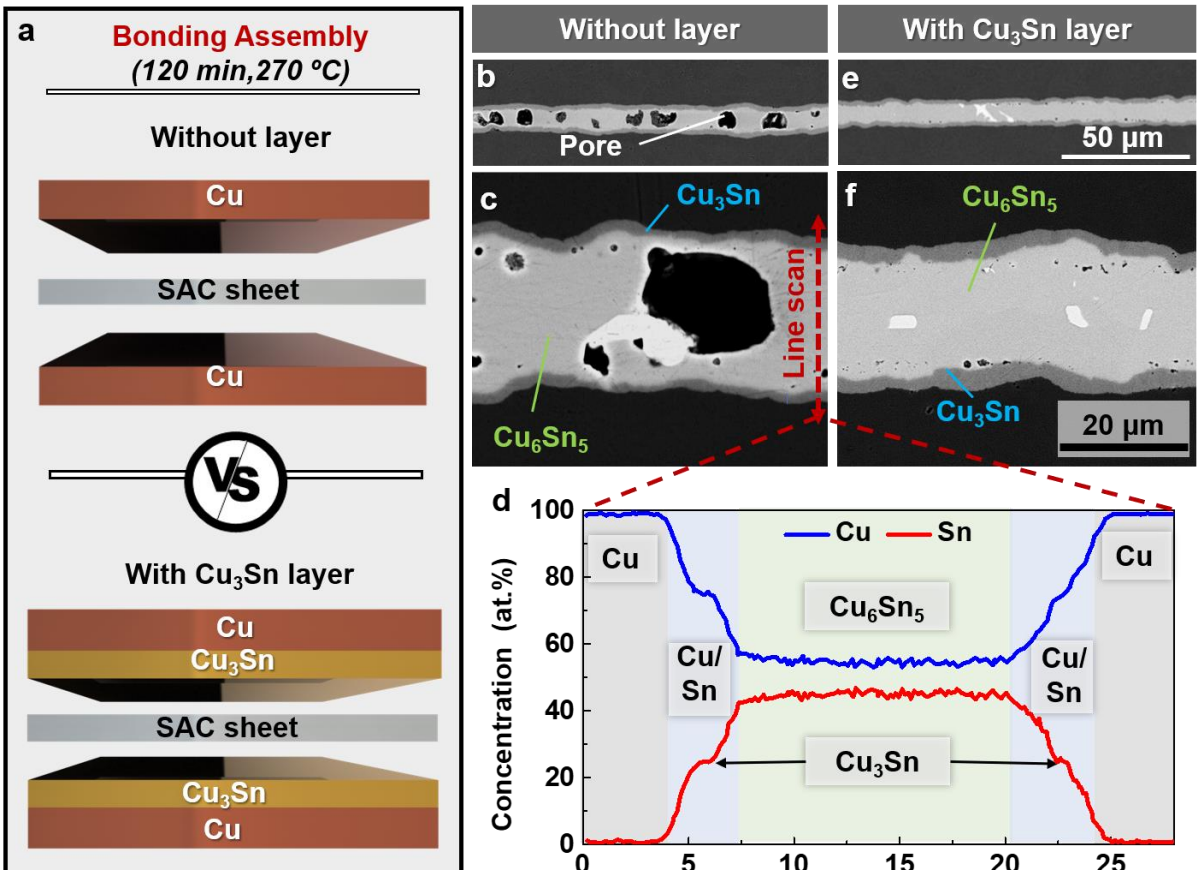

Figure 2. (a) Illustration of the Cu-Sn soldering having or not the Cu_3Sn coated layer, **(b)** and **(c)** Low and high magnifications BSE micrographs of the solder joint formed without the Cu_3Sn coated layer, **(d)** AES line profile across the solder joint and Cu substrates, and **(e)** and **(f)** Low and high magnifications BSE micrograph of the IMC joint formed with the Cu_3Sn coated layer.

3. Microstructural evolution of the Cu-SAC soldering having or not a Cu_3Sn coating layer during the TLP process.

To understand the effect of the Cu_3Sn coated layer on phase evolutions and pore formation, the bonding process was monitored at different stages of the TLP process. **Figure 3a** shows SEM micrographs of a bonded Cu-SAC-Cu sample at 270 ºC for 0, 30, and 90 min and at a constant pressure of 10 kPa. It can be observed that during the heating ramp (t = 0 min) and without the Cu_3Sn coated layer, Cu_6Sn_5 scallops nucleated at the Cu-$Sn_{(l)}$ interfaces. Next, the scallops grew (t = 30 min) until they intercepted the grains from the opposite bonding front (t = 90 min) and

formed a layer across the initial SAC. However, the synthesized Cu_6Sn_5 bonding layer is mixed with unreacted SAC domains. O. Y. Liashenko et al. observed a similar discontinuous Cu_6Sn_5 layer and assimilated it to the scallop grains impingement [19].

On the contrary, for the Cu-Cu_3Sn-SAC-Cu_3Sn-Cu bonded sample (i.e., Cu_3Sn coating on Cu), the reaction between the Cu_3Sn coated layer and $Sn_{(l)}$ led to preferential Cu_6Sn_5 grains nucleation within the liquid. The reaction occurred as early as Sn tuned liquid (t = 0 min). The coalescence of the Cu_6Sn_5 crystal (t = 30 min) produced a uniform and continuous layer across the solder joint (t = 90 min). Only residual SAC can be observed in the vicinity of the Cu_3Sn layer, as shown in **Figure 3b**.

In addition, the Cu_6Sn_5 nuclei in Sn are faceted crystals, which significantly differ from the scallop grains at the Cu/$Sn_{(l)}$ interfaces (**Figure 3a** and **Figure 3b**). The top of the SAC layer was thus etched to gain more insight into the growth of the faceted grains, as illustrated in **Figure 3c**. It is observed that the grains have a polyhedron structure with a hexagonal base, as shown in **Figure 3d**. The morphology of the crystal matches Wulff's construction (**Figure 3e**).

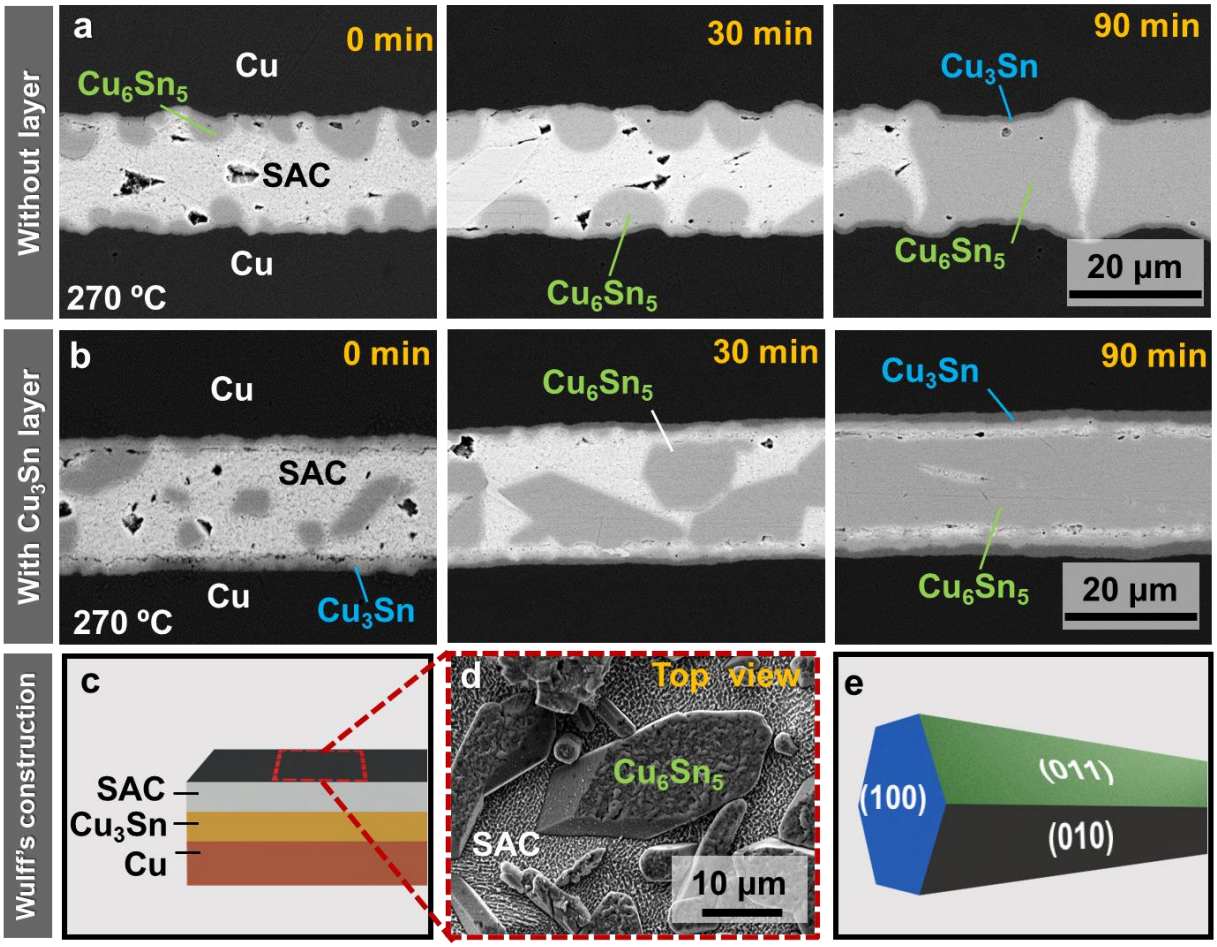

Figure 3. (a) BSE micrographs of the Cu-SAC-Cu bonded samples at 270 ºC and 10 kPa for 0, 30, and 90 min, **(b)** the Cu-Cu_3Sn-SAC-Cu_3Sn-Cu bonded samples, **(c)** illustration of the IMC joint, **(d)** BSE micrograph of the etched Cu-Cu_3Sn-SAC-Cu_3Sn-Cu joint top surface after 15 min at 270 ºC, and **(e)** corresponding Wulff's construction of the Cu_6Sn_5 crystals.

In the previous section, we observed that a Cu_3Sn layer deposited onto the Cu substrate altered the growth of Cu_6Sn_5 grains. Instead of growing in scallops, the Cu_6Sn_5 phase grew in faceted crystals inside the $Sn_{(l)}$. AES maps and line profiles were performed across the Cu-SAC and Cu-Cu_3Sn-SAC interfaces after being heated at 270 ºC for 10 min and under 10 kPa, to understand the role of the Cu_3Sn coated layer on the Cu_6Sn_5 growth mechanisms as shown in **Figure 4a**.

The comparison of AES maps (**Figure 4b**) and line profiles (**Figure 4c**) of the bonded samples show, in both cases, the presence of a ~ 1 µm thick Cu_3Sn interphase and Cu_6Sn_5 scallops. In other words, the Cu_3Sn coated layer does not prevent the growth of Cu_3Sn interphases during the TLP process and does not suppress the scallop grains but restricts their nucleation and growth. The Cu line profile in **Figure 4c** shows that owing to the Cu_3Sn coated layer; the scallop size is fewer than 0.5 µm. Conversely, without the Cu_3Sn coated layer, the scallops developed for more than 1 µm.

Additionally, a smooth transition between Cu_6Sn_5 and Sn is observed in the absence of the Cu_3Sn coated layer. This transition suggests forming a metastable diphasic domain with a high-volume fraction of Cu_6Sn_5 and implies nucleation in progress from Cu to liquid SAC (**Figure 4c**). On the contrary, with a Cu_3Sn coated layer, a sharp transition between Cu_6Sn_5 and Sn is observed suggesting the termination of scallop nucleation at the Cu-$Sn_{(l)}$ interfaces and promoting Cu_6Sn_5 crystal growth in liquid SAC.

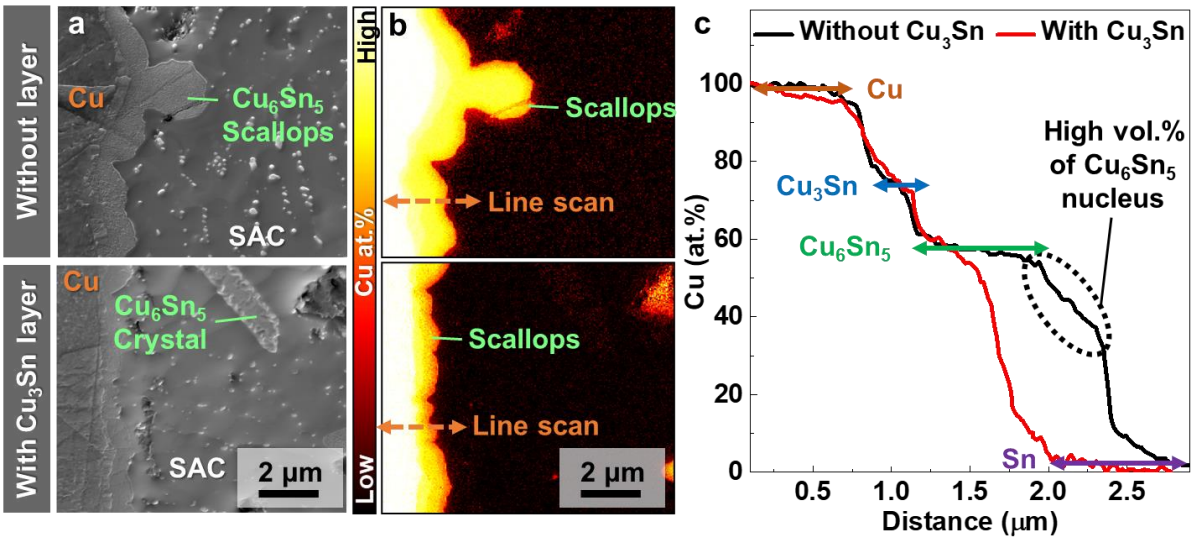

Figure 4. (a) SEM micrograph of the Cu-SAC and Cu-Cu_3Sn-SAC interfaces elaborated at 270 °C for 10 min, **(b)** AES maps of the solder joints, and **(c)** AES line profiles at the Cu-SAC interfaces with and without the Cu_3Sn coated layer.

4. The bonding mechanism of Cu-SAC joints having or not the Cu_3Sn coated layer.

The microstructural, elemental, and chemical analysis of the Cu-SAC bonding via the TLP process and previous studies were then correlated to propose a bonding mechanism, including the Cu_3Sn coated layer effect. Note that the following mechanisms rely on the experimental analysis presented in this paper and previously published kinetics and thermodynamics simulations [8]. The simulations are based upon Fick's diffusion law of the different elements and phases present in the bonding process and corroborated to interfacial mass transport equations. Herein, these mechanisms are used to explain the phase evolutions, pore formation, and the effect of a Cu_3Sn coated layer pre-exists.

In the early stage of the bonding process (t = 0 min), the phases in contact with $Sn_{(l)}$ dissolve (i.e., Cu or Cu_3Sn), supersaturating $Sn_{(l)}$ with Cu (pathway 1). Under these metastable conditions, Cu_6Sn_5 grains nucleate and grow, as illustrated in **Figure 5a-1** and **Figure 5a-2**. However, the nucleation, growth, and morphology of the Cu_6Sn_5 are severely altered by the Cu_3Sn coated layer. In the absence of a Cu_3Sn coated layer, Cu_6Sn_5 scallops nucleate at the $Cu/Sn_{(l)}$ interfaces (**Figure 3a**), while with a Cu_3Sn coated layer, Cu_6Sn_5 faceted crystals nucleate preferentially within $Sn_{(l)}$ (**Figure 3b**). These different growth mechanisms result from a faster Cu dissolution from Cu_3Sn than from pure Cu in $Sn_{(l)}$, as reported by Liashenko et al. [18]. Hence, a low dissolution/nucleation ratio promotes the growth of Cu_6Sn_5 scallops in the vicinity of the dissolving interfaces. On the contrary, a high dissolution/nucleation ratio encourages the development of Cu_6Sn_5 faceted crystals within $Sn_{(l)}$. Naturally, with the Cu_3Sn coated layer, the growth of Cu_6Sn_5 nuclei is faster in $Sn_{(l)}$ than at the $Cu/Sn_{(l)}$ interfaces, giving rise to a grain size discrepancy in the early stage of the bonding process as observed in **Figure 4b** and **Figure 4c**.

After 30 min, Cu_6Sn_5 and Cu react to form a thin Cu_3Sn layer where it was not yet present, as illustrated in **Figure 5b-1**. Then, Cu_6Sn_5 grains grow under a quasi-saturation condition via

grain boundary (pathway 2) and volume (pathway 3) diffusions, as demonstrated by S. Bordère et al. [8]. The diffusion mechanisms generate a transport of species (pathway 1) and vacancies (pathway 4) in $Sn_{(l)}$, which then drive the growth of Cu_6Sn_5 and the formation of pores, respectively. Later, the pressure applied to the sample (i.e., 10 kPa) allows filling pores created during the transport of vacancies. Additionally, the Oswald ripening is another mechanism favoring Cu_6Sn_5 faceted crystal growth within the $Sn_{(l)}$. In both cases, grain boundary and volume diffusions are the limiting mechanisms and related to Cu_6Sn_5 growth. In other words, a similar volume fraction of Cu_6Sn_5 must be obtained regardless of the presence of the Cu_3Sn coated layer and matches our previous volume fraction measurement in **Figure 3a** and **Figure 3b**.

Then, large Cu_6Sn_5 grains coalesce and produce an IMC layer (t = 90 min). Without the Cu_3Sn coated layer, an early grain impingement occurs because of the Cu_6Sn_5 scallops growth from both bonding sides. Later, this impingement constrains the further development of Cu_6Sn_5 into a fixed volume, creating pores where the liquid phase remains (**Figure 3a** and **Figure 5c-1**). On the contrary, with the Cu_3Sn coated layer, the growth of Cu_6Sn_5 arises inside $Sn_{(l)}$, avoiding grain impingement and volume restriction, thus preventing pores (**Figure 3b** and **Figure 5c-2**). Finally, after $Sn_{(l)}$ consumption, Cu_3Sn grows at the detriment of the previously formed Cu_6Sn_5 (120 min). The phase evolution is driven by volume diffusion in which pores size and distribution are unaffected. As a result, without the Cu_3Sn coated layer, the IMC has macro-pores (**Figure 3a** and **Figure 5d-2**), whereas, with the Cu_3Sn coated layer, the IMC is pore-free (**Figure 3b** and **Figure 5d-2**).

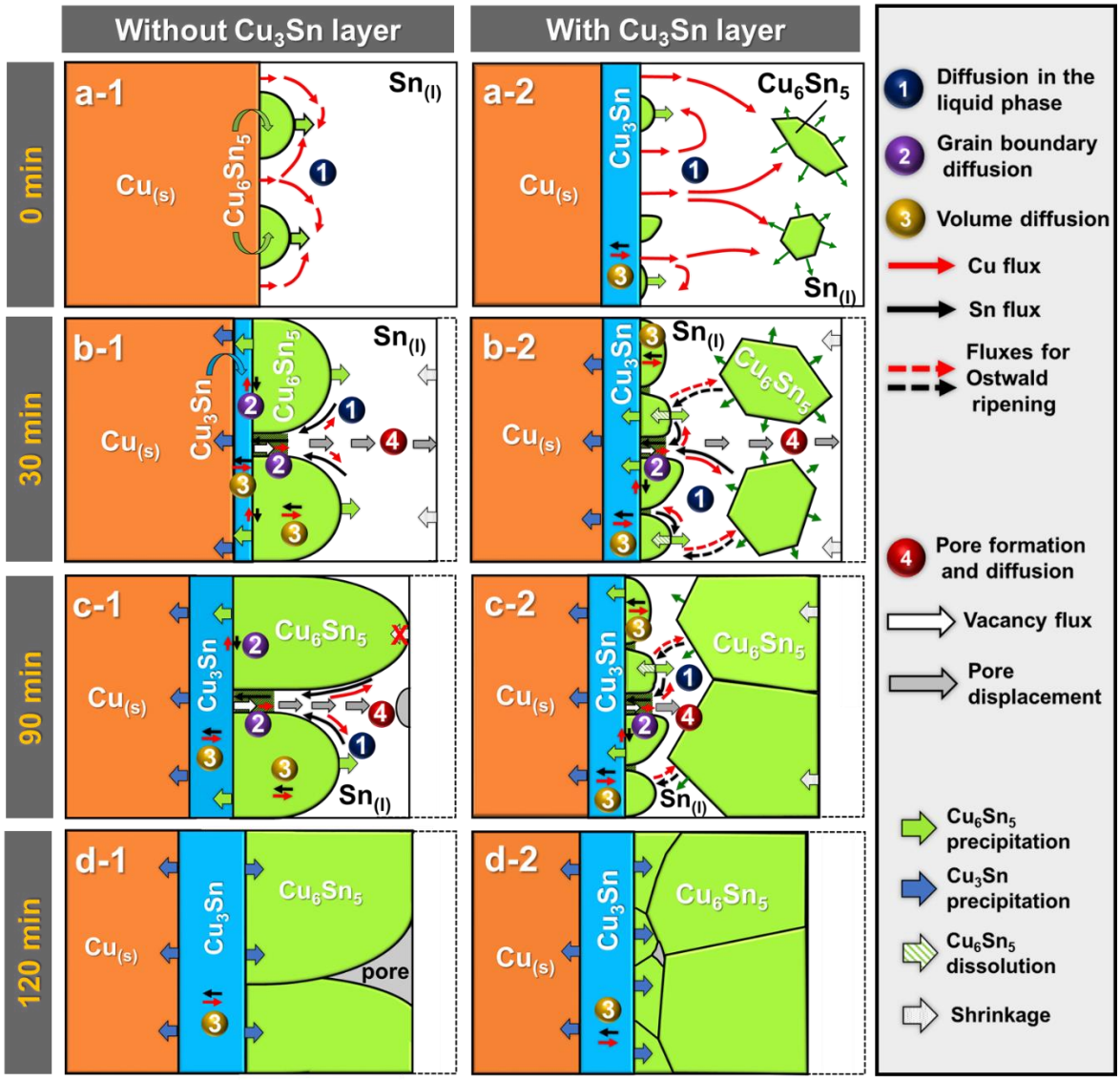

Figure. 5. Illustrations of the Cu-SAC bonding during the TLP process having (column 1) or not (column 2) the Cu_3Sn coated layer after **(a-1)** - **(a-2)** 0 min, **(b-1)** - **(b-2)** 30 min, **(c-1)** - **(c-2)** 90 min, and **(d-1)** - **(d-2)** 120 min.

5. Comparison of the mechanical and thermomechanical properties of TLP and classical Cu-SAC soldering.

The mechanical properties of the developed TLP joints (**Figure 6a**) were then tested and compared to traditional soldering. Two TLP joints were made with a SAC sheet and are composed of either a Cu_6Sn_5 layer having Cu_3Sn interphases (**Figure 6b**) or a fully reacted Cu_3Sn layer (**Figure 6c**). On the other hand, the classical solder was elaborated using a SAC

paste, as illustrates in **Figure 6d**. The use of a solder past led to a 100 µm thick SAC seal, in which Cu_6Sn_5 scallops grew at the Cu/SAC interfaces due to the absence of a Cu_3Sn coated layer as shown in **Figure 6e**.

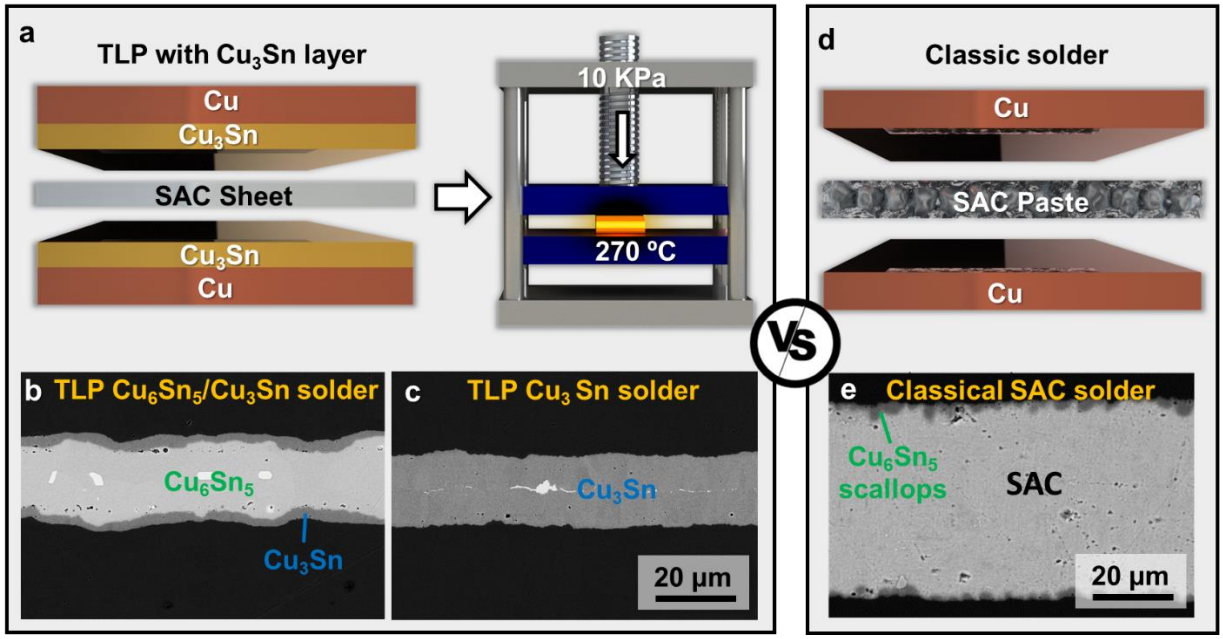

Figure 6. (a) Illustration of the TLP solder having : **(b)** Cu_6Sn_5 layer with Cu_3Sn interphases and **(c)** a Cu_3Sn layer. **(d)** Illustration of the classical solder assembly, and **(e)** BSE micrograph of the classical SAC joint.

The mechanical properties of the joints were measured via DNS test, as illustrated in **Figure 7a.** The test consists of creating two notches perpendicular to the IMC and on each side of the Cu substrates. Then, a force is applied to the top of the assembly. The applied force makes the joint's surface between the notches under shear stresses, as shown in **Figure 7b**, causing the notches to break and close.

Figure 7c shows the results of the DNS test for the different bonded layers. As can be observed, the classical SAC has a plastic deformation, followed by its failure at 40 MPa. Above 40 MPa cracks arose along the Cu-SAC interphase, leading to the SAC delamination from the Cu substrate, as shown in **Figure 7d**. Next, the TLP Cu_3Sn /Cu_6Sn_5/Cu_3Sn solder joint presents a brittle fracture above 35 MPa, causing its failure. However, the TLP Cu_3Sn solder joint does

not show a fracture at the end of the DNS test. The stress increased linearly with displacement producing a plastic deformation above 80 MPa, leading to the notches closure by Cu deformation. As shown in **Figure 7e**, the TLP Cu_3Sn joint cracked vertically and did not propagate in Cu because of its high toughness, allowing thus to prevent the delamination of the assembly by accommodating the deformations.

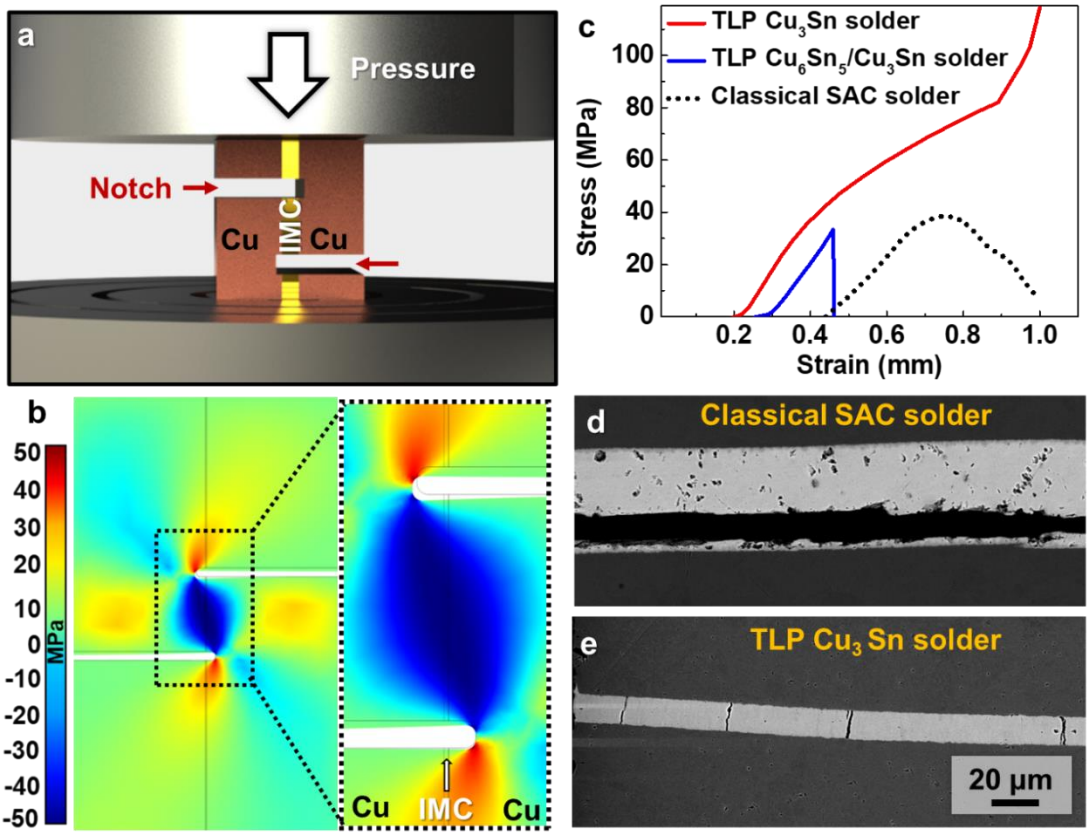

Figure 7. (a) Schematic of the DNS test and **(b)** simulation of the stresses induced during the DNS test, and **(c)** stress vs. strain curves of bonded samples. BSE micrographs after the DNS test of **(d)** reference SAC and **(e)** Cu_3Sn with a pre-existing Cu_3Sn layer.

The reliability of the solder joint depends upon the number of thermal cycles it can endure. Heating and cooling an electronic module create thermal stresses at the joint/metal interface leading to delamination and failure. Also, thermal stresses are significant when materials on both sides of the soldering have different coefficients of thermal expansion (CTE). Therefore,

to generate sufficient thermal stresses in the assembly during thermal cycling, Cu matrix composites were fabricated and bonded. One side of the assembly is composed of a Cu matrix reinforced with 30 vol.% of CFs, while the other side is composed of a Cu matrix reinforced with 40 vol.% of CFs, as illustrated in **Figure 8a**. The CTEs of the Cu/30 vol.% CFs and Cu/40 vol% CFs composites are 14.10^{-6} K^{-1} and 10.10^{-6} K^{-1}, respectively. A 100 μm Cu layer was placed between the composite and SAC to assure the bonding. Once bonded, the assemblies were inserted in a climatic chamber and subjected to open-air passive thermal cycles, as illustrated in **Figure 8a**. The duration of a cycle was set 120 min, with a first plateau at 180 °C for 20 min and a second plateau at -45 °C for 20 min.

Figure 8b presents the mechanical shear behavior of the Cu-Cu_3Sn-Cu_6Sn_5-Cu_3Sn-Cu TLP and classical solder after 0, 500, and 1200 thermal cycles. It can be observed that the mechanical shear resistance of classical SAC joint decreases from 30 MPa at t_0 to 6 MPa at t_{1200}, corresponding to an 80 % decrease in resistance. **Figure 8c** shows that cracks formed inside the solder joint, and delamination occurred after only 500 thermal cycles. In opposition, the TLP joint has a resistance of up to 45 MPa with a minor decrease of its mechanical resistance after 1200 cycles. The slight tensile strength reduction from 45 to 35 MPa is attributed to decreased Cu/CFs composite shear strength (CTE mismatch between Cu and CFs). **Figure 8d** shows SEM micrographs of the TLP solder layer after 0, 500, and 1200 cycles. It can be noticed that after 500 cycles, the initial Cu_6Sn_5 layer transformed to Cu_3Sn, and the joint is free of defects. The successive deformation of the composite assembly during the cycling generates vertical cracks, as seen during the DNS test. The vertical cracks allow withstanding significant thermomechanical stresses and thus preserving the assembly integrity. The IMCs assemblies manufactured with the Cu_3Sn coated layer possess then excellent thermal cycling reliability.

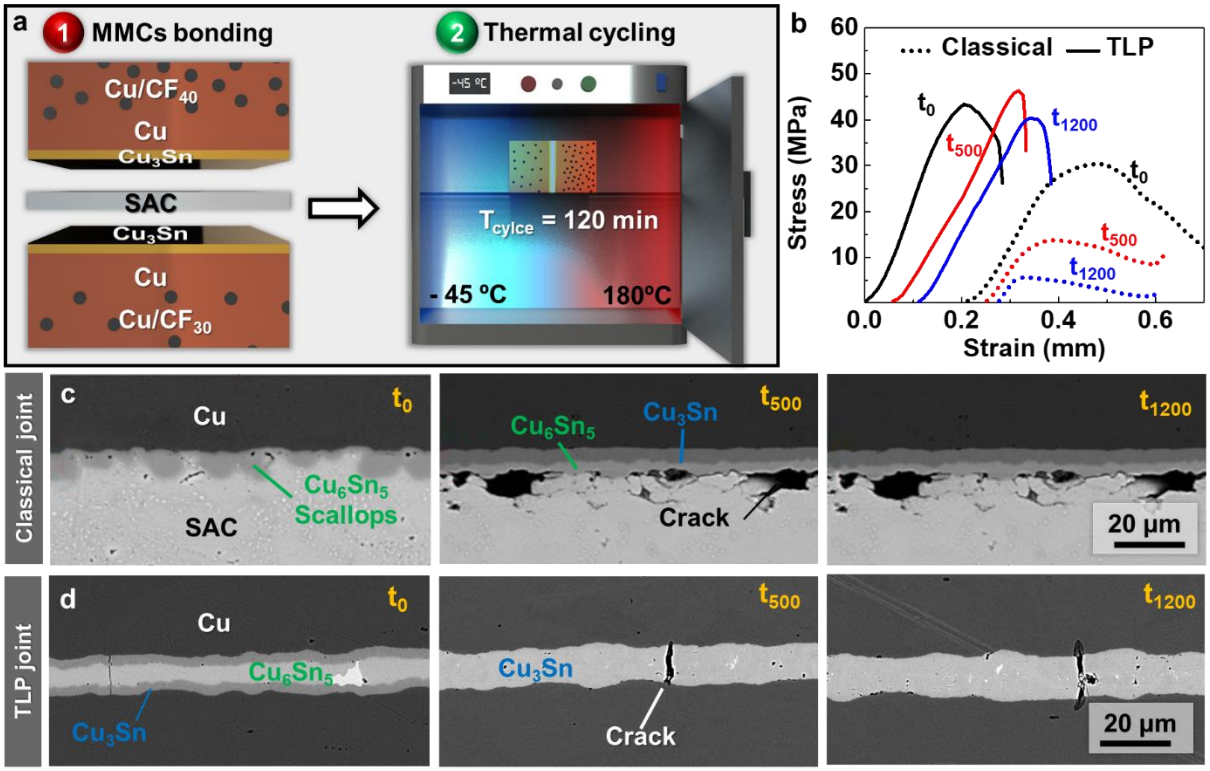

Figure 8. **(a)** Illustration of the thermal cycling process of bonded Cu/CF(40 vol.%) - Cu/CF(30 vol.%) composites, **(b)** Strain-stress curves of the composite assemblies as a function of the number of thermal cycles for TLP and classical soldering **(c)** BSE micrographs of the classical SAC bonding composites as a function of the number of thermal cycles (0, 500, 1200 cycles), and **(d)** TLP soldering for different thermal cycles.

Conclusion

In summary, we showed that adding a Cu_3Sn coated layer between Cu and SAC positively altered the nucleation, growth, and morphology of IMCs during the TLP soldering process. The Cu_3Sn coated layers restrained the growth of Cu_6Sn_5 scallops in the vicinity of the Cu_3Sn-SAC interfaces avoiding scallops grains impingement and pores formation. We argued that inserting a Cu_3Sn layer between permitted a fast dissolution of Cu in $Sn_{(l)}$, promoting Cu_6Sn_5 nucleation within $Sn_{(l)}$, rather than at the $Cu/Sn_{(l)}$ interfaces, thereby forming a dense, robust and reliable joint. As demonstrated, the TLP solder having a Cu_3Sn layer withstood more than 80 MPa and

1200 thermal cycles from -45 to 180 ºC without delaminating from Cu, making it stronger and steadier than a classical SAC solder, which cracked when subjected to more than 45 MPa and 500 cycles. Our approach of modifying the interfacial exchange during liquid soldering will open pathways toward the fabrication of high-power densities IMCs joint and will advance strategies of enhancing power module performances.

Author information

Corresponding Author

*Corresponding author: Institut de Chimie de la Matière Condensée de Bordeaux, ICMCB-CNRS, 87 Avenue du Dr A. Schweitzer, F-33608 PESSAC Cedex, France.
Phone: +33 (0)5 40 00 84 37
Email address: jean-francois.silvain@icmcb.cnrs.fr

Author Contributions

The manuscript was written through contributions of all authors. All authors have given approval to the final version of the manuscript.

Funding Sources

No funding sources

Abbreviations

TLP, transient liquid phase; IMC, intermetallic compound; Cu, Copper; Sn, Tin; SEM, scanning electron microscope; SAC, $SnAg_{3.8}Cu_{0.7}$; AES, Auger electron spectroscopy; BSE, back scattered electron; $Sn_{(l)}$, liquid tin; DNS, Double notch shear; CTE, coefficient of thermal expansion; CFs, carbon fibers.

References

[1] Kassakian, J.; Perreault, D. The future of electronics in automobiles 13th International Symposium on Power Semiconductor Devices and ICs (ISPSD 01), 2001.

[2] Madjour, K. Silicon Carbide market update: from discrete devices to modules PCIM Europe 2014, Nuremberg.

[3] Lynch, J. F. Brazing by the Diffusion-Controlled Formation of a Liquid intermediate Phase Welding Journal 1959, 38(2) 85-89.

[4] Jung, D.; H., Sharma, A.; Mayer, M.; Jung, J.P. A Review on Recent Advances in Transient Liquid Phase (TLP) Bonding for Thermoelectric Power Module Reviews on advanced materials science 2018, Volume 53: Issue 2, 147-160.

[5] Li, J.F. Interfacial reaction in Cu/Sn/Cu system during the transient liquid phase soldering process P.A. Agyakwa, C.M. Johnson Acta Mater. 2011, 59, 1198-1211.

[6] Harris, J.; Matthews, M. Selecting Die Attach Technology for High-Power Applications Power Electronics Technology 2009, 35(11), 18-23.

[7] Heuck, N.; Guth, K.; Thoben, M.; Müller, A.; Oeschler, N.; Böwer, L.; Speckels, R.; Krasel, S.; Ciliox, A. Aging of new Interconnect-Technologies of Power-Modules during Power-Cycling", CIPS Nuremberg, 2014

[8] Bordère, S.; Feuillet, E.; de Langlade, R.; Diot, J.L.; Silvain, J.F. Understanding of void formation in Cu/Sn-Sn/Cu system during transient liquid phase bonding process through diffusion modeling Metallurgical and Materials Transactions B 2018 Volume 49, 3343–3356.

[9] Chin, C.; Lee, P.; Wang, J.; Jong, S. Are Intermetallic in Solder Joints Really Brittle? Electronic Components and Technology Conference, 2007

[10] Massalski, T.B. Binary alloy phase diagrams, ASM Int. Materials Park, Ohio 1990, 1481-1483

[11] Fürtauer, S.; Li, D.; Cupid, D.; Flandorfer, H. The Cu–Sn phase diagram, Part I: New experimental results Intermetallics 2013, 34, 142-147.

[12] Heuck, N.; Guth, K.; Thoben, M.; Müller, A.; Oeschler, N.; Böwer, L.; Speckels, R.; Krasel, S.; Ciliox, A. Aging of new Interconnect-Technologies of Power-Modules during Power-Cycling CIPS Nuremberg, 2014.

[13] Flötgen, C.; Pawlak, M.; Pab, E. Wafer bonding using Cu–Sn intermetallic bonding layers Microsyst. Technol. 2014, 20, 653-662.

[14] Chui, W.L.; Liu, C.M.; Haung, Y.S.; Chen, C. Formation of nearly void-free Cu_3Sn intermetallic joints using nanotwinned Cu metallization Appl. Phys. Lett. 2014, 104, 171902.

[15] Ma, D.; Wang, W.D.; Lahiri, S.K. Scallop formation and dissolution of Cu–Sn intermetallic compound during solder reflow J. Appl. Phys. 2002, 91, 3312-331.

[16] Bosco, N.S.; Zok, F.W. Critical interlayer thickness for transient liquid phase bonding in the Cu–Sn Acta Mater. 2004, 52, 2965-2972.

[17] Brincker, M.; Sohl, S.; Eisele, R.; Popock, V.N. Strength and reliability of low temperature transient liquid phase bonded Cu-Sn-Cu interconnects Microelectronics Reliability 2017, 76-77, 378-382.

[18] Mokhtari, O. A review: Formation of voids in solder joint during the transient liquid phase bonding process – Causes and solutions Microelectronics Reliability 2019, 98 95-105.

[19] Liashenko, O.Y.; Gusack, A.M.; Hodaj, F. Phase growth competition in solid/liquid reactions between copper or Cu_3Sn compound and liquid tin-based solder J. Mater. Sci.: Mater. Electron 2014, 25, 4664-4672.

[20] Liashenko, O.Y.; Hodaj, F. Initial stage of isothermal wetting of bulk Cu_6Sn_5, Cu_3Sn and Cu substrates by liquid Sn J. Mater. Sci.: Mater. Electron 2019, 30, 1838–1849.

[21] Feuillet, E. PhD thesis, Bordeaux University, March 2016.

Figure legend:

Figure 1. (a) Illustration of the Cu_3Sn coated layer synthetized on Cu. SEM micrographs of the Cu_3Sn, **(b)** top, and **(c)** cross-sectional views.

Figure 2. (a) Illustration of the Cu-Sn soldering having or not the Cu_3Sn coated layer, **(b)** SEM micrographs of the solder joint formed without the Cu_3Sn coated layer, **(c)** AES line profile across the solder joint and Cu substrates, and **(d)** SEM micrograph of the IMC joint formed with the Cu_3Sn coated layer.

Figure 3. (a) SEM micrographs of the Cu-SAC-Cu bonded samples at 270 ºC and 10 kPa for 0, 30, and 90 min, **(b)** the Cu-Cu_3Sn-SAC-Cu_3Sn-Cu bonded samples, **(c)** illustration of the IMC joint, **(d)** SEM micrograph of the etched Cu-Cu_3Sn-SAC-Cu_3Sn-Cu joint top surface after 15 min at 270 ºC, and **(e)** corresponding Wulff's construction of the Cu_6Sn_5 crystals.

Figure 4. (a) SEM micrograph of the Cu-SAC and Cu-Cu_3Sn-SAC interfaces elaborated at 270 °C for 10 min, **(b)** AES maps of the solder joints, and **(c)** AES line profiles at the Cu-SAC interfaces with and without the Cu_3Sn coated layer.

Figure**. 5.** Illustrations of the Cu-SAC bonding during the TLP process having (column 1) or not (column 2) the Cu_3Sn coated layer after **(a-1)** - **(a-2)** 0 min, **(b-1)** - **(b-2)** 30 min, **(c-1)** - **(c-2)** 90 min, and **(d-1)** - **(d-2)** 120 min.

Figure 6. (a) Illustration of the TLP solder having: **(b)** Cu_6Sn_5 layer with Cu_3Sn interphases and **(c)** a Cu_3Sn layer. **(d)** Illustration of the classical solder assembly, and **(e)** SEM micrograph of the classical SAC joint.

Figure 7. (a) Schematic of the DNS test and **(b)** simulation of the stresses induced during the DNS test, and **(c)** stress vs. strain curves of bonded samples. SEM micrographs after the DNS test of **(d)** reference SAC and **(e)** Cu_3Sn with a pre-existing Cu_3Sn layer.

Figure 8. **(a)** Illustration of the thermal cycling process of bonded Cu/CF(40 vol.%) - Cu/CF(30 vol.%) composites, **(b)** Strain-stress curves of the composite assemblies as a function of the number of thermal cycles for TLP and classical soldering **(c)** SEM micrographs of the classical SAC bonding composites as a function of the number of thermal cycles (0, 500, 1200 cycles), and **(d)** TLP soldering for different thermal cycles.

Graphical abstract: